Turbulence Appearance and Nonappearance in Thin Fluid Layers

Gregory Falkovich[1,2,3] and Natalia Vladimirova[4]
[1]Weizmann Institute of Science, Rehovot 76100, Israel
[2]Institute for Information Transmission Problems, Moscow 127051, Russia
[3]Novosibirsk State University, 630090 Novosibirsk, Russia
[4]University of New Mexico, Albuquerque 87131, New Mexico, USA

(Received 20 February 2018; published 16 October 2018)

Flows in fluid layers are ubiquitous in industry, geophysics, and astrophysics. Large-scale flows in thin layers can be considered two dimensional with bottom friction added. Here we find that the properties of such flows depend dramatically on the way they are driven. We argue that a wall-driven (Couette) flow cannot sustain turbulence, no matter how small the viscosity and friction. Direct numerical simulations (DNSs) up to the Reynolds number $\mathrm{Re} = 10^6$ confirm that all perturbations die in a plane Couette flow. On the contrary, for sufficiently small viscosity and friction, perturbations destroy the pressure-driven laminar (Poiseuille) flow. What appears instead is a traveling wave in the form of a jet slithering between wall vortices. For $5 \times 10^3 < \mathrm{Re} < 3 \times 10^4$, the mean flow in most cases has remarkably simple structure: the jet is sinusoidal with a parabolic velocity profile, and vorticity is constant inside vortices, while the fluctuations are small. At higher Re, strong fluctuations appear, yet the mean traveling wave survives. Considering the momentum flux barrier in such a flow, we derive a new scaling law for the Re dependence of the friction factor and confirm it by DNS.

DOI: 10.1103/PhysRevLett.121.164501

A century and a half of ever-expanding studies of turbulence onset in three-dimensional channel and pipe flows has brought a wealth of fundamental and practical knowledge; see, e.g., Ref. [1] and references therein. The wall-driven flow is linearly stable, while the flow driven by pressure gradient or other bulk force can be unstable for large enough values of the Reynolds number (Re) [2,3]. Notwithstanding this difference and irrespective of linear stability, all flows undergo the transition to turbulence at sufficiently high Re when finite-amplitude perturbations persist [1]. Some perturbations can take the form of traveling waves of finite amplitude [4–6], yet all patterns are unstable and transient, so the 3D flow is quite irregular already at moderate Re [1,7].

In contrast, for quasi-two-dimensional channel flows, it is not even known if they are able to produce turbulence at all. This is despite a rapidly expanding interest motivated by the needs of industry, astrophysics, geophysics, and laboratory experiments in fluid layers and soap films (see, e.g., Refs. [8,9], the recent collection [10], and the references therein). To the best of our knowledge, in all experiments in layers and films, external forces and obstacles were needed to produce turbulence (see, e.g., Ref. [11]), and it is not known if such turbulence is able to sustain itself in a channel flow past an obstacle. The reason is that 2D ideal hydrodynamics conserves energy (squared velocity) and enstrophy (squared vorticity). Force at intermediate scales can generate two-cascade turbulence with energy (enstrophy) cascading upscale (downscale). On the contrary, in a wall or pressure-driven flow, the input is at the largest scale, so that it is *a priori* unclear what kind of turbulence, if any, can exist in the limit of low viscosity and friction.

Combining analytic theory and direct numerical simulation (DNS), we answer here this fundamental question. We describe how turbulence appears and develops in pressure-driven flows: as a "snake" traveling wave—a jet meandering between counterrotating vortices and preserving its form even for strong fluctuations; see Fig. 1. Even more remarkably, we find that wall-driven flows relax to the laminar state for all values of viscosity and friction used, and they remain laminar for as long as we are able to follow. Both findings substantially widen our fundamental perspective on turbulence and may lead to diverse practical applications.

We start our consideration by analyzing the interplay between momentum and vorticity averaged along the channel. Convection carries vorticity unchanged, while viscosity diffuses it, so that any turbulence must lead to vorticity mixing and homogenization. We thus expect the mean cross-channel vorticity profile in a turbulent flow (outside a viscous wall layer) to be more flat than the laminar profile. On the other hand, turbulence transfers momentum to the walls faster than a laminar flow, thus increasing the drag and decreasing the mean velocity. Averaged along the channel, vorticity is the transverse derivative of the velocity. The requirements on momentum and vorticity profiles are compatible for pressure-driven

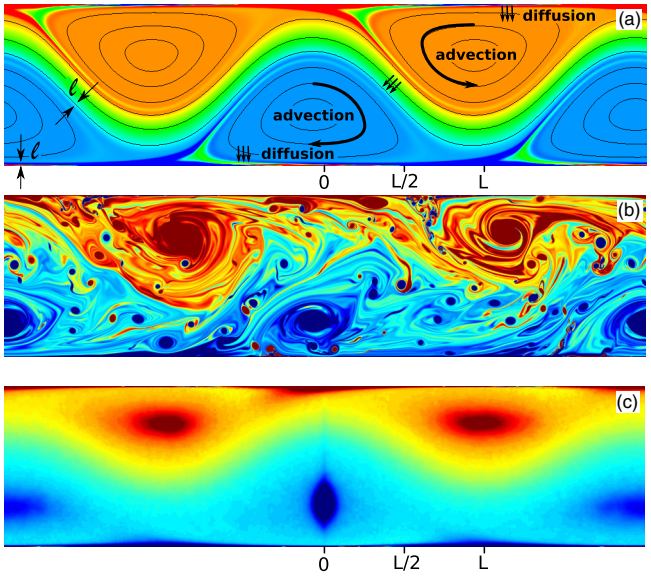

FIG. 1. Vorticity snapshot for pressure-driven flows at (a) $\mathrm{Re} = 1.42 \times 10^4$ with streamlines. (b) Vorticity at $\mathrm{Re} = 2.94 \times 10^5$. (c) Vorticity averaged over 7000 snapshots (distance $1400L$) in the frame of the negative vortex for $\mathrm{Re} = 2.94 \times 10^5$.

flows where turbulence flattens both the velocity and vorticity profiles. On the contrary, the mean velocity profile is monotonic for wall-driven flows, so decreasing velocity in the bulk while keeping it at the walls would make the vorticity profile more nonuniform. We then conclude that the momentum and vorticity requirements on turbulence in 2D wall-driven flows are contradictory.

For a more formal argument, consider the 2D Navier-Stokes equation with unit density and a uniform friction rate α:

$$\partial_t \boldsymbol{v} + (\boldsymbol{v}\cdot\nabla)\boldsymbol{v} = \nu\Delta\boldsymbol{v} - \nabla p - \alpha\boldsymbol{v}, \quad \nabla\cdot\boldsymbol{v} = 0. \tag{1}$$

Already for the frictionless case (relevant, e.g., for flows on superhydrophobic surfaces [12] or soap films under low air pressure), a dramatic difference from the 3D case follows from the relation between momentum and vorticity fluxes, unique for two dimensions. Denote u, v the fluctuating velocity components respectively parallel and perpendicular to the walls, which are placed at $y = \pm L/2$ and move with $\pm V/2$. Let us average the x component of Eq. (1) with $\alpha = 0$ both over time and over x (zonally). The result can be written using vorticity, $\omega = \nabla \times \boldsymbol{v}$:

$$\partial_y(\nu\Omega + \langle uv\rangle) = \nu\Omega_y - \langle v\omega\rangle = \langle\nabla p\rangle. \tag{2}$$

Here $\Omega(y)$ is the vorticity averaged over time and x. Turbulence adds extra fluxes of x momentum and vorticity, related by the Taylor theorem: $\partial_y\langle uv\rangle = -\langle v\omega\rangle$. When $\langle\nabla p\rangle = 0$, the first part of Eq. (2) gives the constancy of the cross-flow momentum flux, whose direction is set by viscosity at the wall. On the other hand, the second part of Eq. (2) gives $\langle v\omega\rangle = \nu\Omega_y$—that is, the existence of turbulence would absurdly mean that the vorticity flux is directed along the mean vorticity gradient. In other words, the right direction of the momentum flux (from large to small values) requires the wrong direction of the vorticity flux (from small to large) in 2D wall-driven flows. In essence, the laminar profile $U = Vy/L$ already has a constant vorticity; one cannot excite turbulence to make it more flat. If we add bottom friction, then the laminar profile gets an inflection point, but it is a vorticity minimum, so that the flow is getting more stable according to the Fjortoft criterium [13]. Indeed, adding to the viscous flow, extra dissipation due to bottom friction could diminish fluctuations but cannot create them.

These nonrigorous but plausible arguments suggest that a wall-driven flow must relax to the laminar state, $U(y) = V\sinh(y\sqrt{\alpha/\nu})/2\sinh(L\sqrt{\alpha/\nu}/2)$, for any ν and α. This is supported by DNSs whose details are described in the Supplemental Material [14]. Starting from different multivortex configurations, we observe different transients and eventual relaxation to the laminar flow in all cases. These results strongly suggest that the laminar wall-driven flow is the global attractor in two dimensions, no matter how small the viscosity and friction. To the best of our knowledge, this is the first such example in the whole fluid mechanics.

From another perspective, the impossibility of turbulence in a 2D wall-driven flow can be related to sign-definite mean vorticity and shear. Even when we initially create vortices of both signs, the vorticity of the sign opposite to the mean is destroyed by the shear, while the same-sign vorticity is homogenized back into the laminar profile. On the contrary, for pressure-driven flows, the mean vorticity has opposite signs at opposite walls, so that turbulence cannot homogenize vorticity back to the laminar profile.

We turn now to pressure-driven flows and define the dimensionless control parameters $\mathrm{Re}_A = A^{1/2}L^{3/2}/\nu$ and $\mathrm{Ru}_A = A^{1/2}/\alpha L^{1/2}$. Here $A = \langle\nabla p\rangle$ is either the mean pressure gradient divided by density or the gravity acceleration for soap films. There is a rich history of modeling 2D Navier-Stokes channel flows—see, e.g., Refs. [3,15,16] and the references therein. In particular, extensively studied were subcritical instability of the laminar flow at $\mathrm{Re}_c = 5772$ (where $\mathrm{Re} = 3L\bar{U}/4\nu$ and $\bar{U}$ is the flow rate) [17] and streamwise localization of the traveling wave at $\mathrm{Re} < \mathrm{Re}_c$ [16]. To the best of our knowledge, the largest, $\mathrm{Re} = 10^4$, was achieved in Refs. [15,18], where transitional turbulence was observed and fully developed turbulence was estimated to appear around 2×10^5, which was beyond computer resources back then. Here we explore higher Re never treated before; we also add uniform friction to relate to real fluid layers.

We focus on a solution that appears from a generic initial condition in a wide interval of Re. To much surprise, we

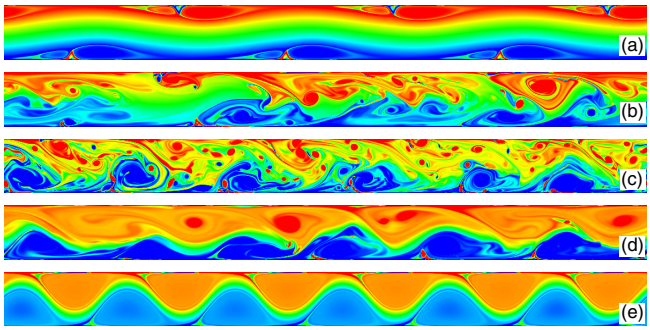

FIG. 2. (a)–(e) Evolution of $12L$ perturbation for $\mathrm{Re}_A = 894$ at $tU_{\mathrm{lam}}/L = 312$, 370, 764, 2199, and 5079, respectively.

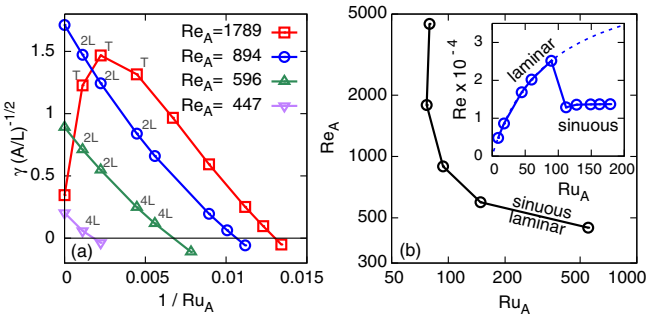

FIG. 3. (a) The growth rate of $4L$ perturbations versus friction for different viscosities. The marks "4L" and "2L" indicate wavelengths of the long-term sinuous flow, and "T" indicates the long-term turbulent flow. (b) Stability diagram in the friction-viscosity space. Inset: Re versus friction.

find that in relatively short channels with periodic boundary conditions, a periodic traveling wave is a long-time attractor at intermediate Re, and even a strongly turbulent state at high Re has the mean profile of such a form (Fig. 1). The transition to the steady state is slow and can be nonmonotonic. In all cases, pressure-driven flows relax to either of two states: the laminar unidirectional flow or a "snake" traveling wave. In the latter case, most of the flux occurs along a sinusoidal jet meandering between two sets of counterrotating vortices rolling along the walls. An example of quite turbulent evolution which results in a remarkably simple flow is shown in Fig. 2. While we cannot rule out switches between the states (as in 3D pipe flow) on an astronomical time scale, we have not seen them once the statistical steady state is established.

The time of transients can be reduced by starting with a low-amplitude perturbation to mimic the naturally developing instability of the laminar flow [2,17]. Then the early evolution shows well-defined exponential growth. Modeling a $12L$ channel, we applied perturbations with the wavelengths $\lambda_{\mathrm{pert}} = 3$, 4, 6, $12L$ for $\mathrm{Re}_A = 894$ and $\mathrm{Ru}_A = 179$. The largest growth rate γ was found for $\lambda_{\mathrm{pert}} = 4L$ and is shown in Fig. 3(a). In the Re_A-Ru_A plane, the $\gamma = 0$ line separates laminar and sinuous flows in Fig. 3(b). The inset in Fig. 3 shows the Reynolds number as a function of Ru_A for $\mathrm{Re}_A = 894$. When friction is large, the flow is laminar. As friction is reduced, the laminar flow becomes faster until it transitions to the sinuous state at $\mathrm{Ru}_A \approx 100$ when the flow rate drops. So, one can speed up the flow by increasing friction, facilitating transition from the sinuous to the laminar regime.

Close to the threshold Re_A, Ru_A, the saturated sinuous flow in the $4L$ and $12L$ channels has the wavelength, $\lambda = 4L$, of the fastest-grown perturbation. At higher Re_A, Ru_A levels, the initial growth of the $4L$ mode is followed by the transition to a shorter wavelength: as Re_A and Ru_A increase, we observe $\lambda = 3L$, $2.4L$, and eventually $2L$. Reducing dissipation further, we observe a sinuouslike flow with strong fluctuations, which we call "turbulence." Figure 3(a) shows the growth rates for $4L$ perturbations, where the marks "4L," "2L," and "T" indicate long-term saturated states in the $4L$ domain.

Let us now take a closer look at these long-term states for frictionless systems. Traveling waves in short channels at intermediate Re were observed before [15,19,20]. Right above Re_c [17], in the interval $5 \times 10^3 \lesssim \mathrm{Re} \lesssim 3 \times 10^4$ ($\mathrm{Re}_A \lesssim 1500$), all saturated flows in the $4L$ channel have a form of sinuous traveling wave with small temporal variations. In the longer $12L$ channel, the moderate-Re runs ($\mathrm{Re} = 14200$, $\mathrm{Re}_A = 894$ and $\mathrm{Re} = 6320$, $\mathrm{Re}_A = 447$) saturate at channel-filling periodic trains, which fit six and five wavelengths, respectively. Closer to the laminar threshold, for $\mathrm{Re} = 4620$ ($\mathrm{Re}_A = 316$), we have observed streamwise localization or train breakdown [16,21], where one out of four pairs of counterrotating vortices was periodically disappearing (see the Supplemental Material [14] for details).

For $400 \lesssim \mathrm{Re}_A \lesssim 1500$, the spatially periodic mean flow in a comoving reference frame has a beautifully simple structure: The jet is sinusoidal with an approximately parabolic velocity profile, while vorticity is essentially constant across each vortex, which appears as a plateau in the vorticity cross sections in Fig. 4(a). Constant vorticity inside the vortices can be explained in the spirit of Ref. [22] as a consequence of viscosity being very small and yet finite: The former means that vorticity must be constant *along* the (closed) streamlines, while the latter means constancy *across* the streamlines in a stationary flow. The same argument suggests the vorticity flux constancy across the jet, so that vorticity changes linearly between opposite values at the separatrices.

At $\mathrm{Re}_A \approx 1500$, the flow becomes turbulent. Chaotic small vortices are created at the walls and swept into a big vortex of the same sign, thus feeding the large-scale flow. For $\mathrm{Re}_A \gtrsim 2000$ and up to 8000 ($\mathrm{Re} = 2.94 \times 10^5$), the relative level of velocity and vorticity fluctuations remains constant within our accuracy. All turbulent flows observed in the $4L$ channel have a pronounced large-scale structure of a jet and a $2L$ periodic chain of vortices, similar to the

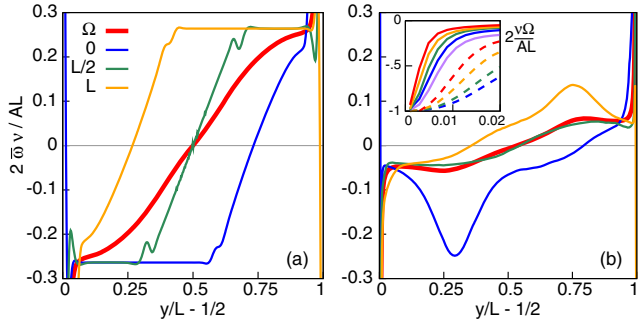

FIG. 4. Vorticity $\bar{\omega}(x,y)$ time-averaged in the moving frame of a vortex. Vertical slices are taken at $x = 0, L/2, L$, as in Fig. 1. (a) $\mathrm{Re}_A = 516$. (b) $\mathrm{Re}_A = 4000$. The red line is zonally averaged vorticity, $\Omega(y) = \int \bar{\omega}(x,y)dx$. Inset: Ω in the boundary layer for $\mathrm{Re}_A = 516$, 362, 894, 1265, 2000, 2828, 4000, 5656, and 8000, from bottom to top.

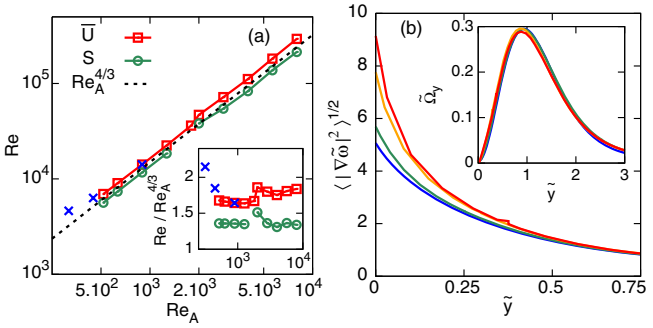

FIG. 5. (a) The Reynolds numbers, based on flow rate $\bar{U}$ and wave speed S, versus pressure (Inset: compensated by $\mathrm{Re}^{4/3}$). Three crosses are for $12L$, while the rest are for the $4L$ channel. (b) Vorticity gradient variance for $\mathrm{Re}_A = 8000$, 5656, 4000, and 2828, from top to bottom, in coordinates $\nabla\tilde{\omega} = \nabla\omega \mathrm{Re}_A^{-2/3}\nu/AL$ and $\tilde{y} = (y/L - 1/2)\mathrm{Re}_A^{2/3}$. Inset: Gradient of Ω.

sinuous flow. This is seen from the comparison of Fig. 1(a) with Fig. 1(c) averaged in the frame of the stronger negative vortex (the other vortices are blurred by fluctuations). While horizontally averaged $\bar{U}, \Omega$ for sinuous and turbulent flows are of similar shape, time averaging exposes a qualitative difference: in the turbulent vortex, the mean vorticity has a peak rather than a plateau; see Figs. 4 and 1.

From the topology of the mean flow, seen in Fig. 1(a), we now derive the relation between the applied force A and the flow rate $\bar{U}$ in the limit of large Re_A. The transfer of momentum (or equivalently vorticity) from the center to the walls encounters two separatrices: one separating the vortex from the jet, and one separating it from the wall layer. Vorticity is diffused by viscosity across the separatrix, and then is carried fast by advection inside the vortex, and then transferred by viscosity towards the wall. There are thus two viscous bottlenecks (transport barriers) in this transfer: on the jet-vortex separatrix and on the wall boundary layer. The width ℓ of the separatrix layer can be estimated by requiring the diffusion time ℓ^2/ν to be comparable to the turnover time L/U, which gives $\ell \simeq (\nu L/U)^{1/2}$ and the effective viscosity $\nu_e \simeq U\ell \simeq \sqrt{\nu UL}$ (we do not distinguish U and $\bar{U}$ in the estimates). The momentum flux due to force must be carried by the viscosity towards the walls, $A \simeq \nu_e U/L^2$, which gives the flow rate and turbulent viscosity:

$$\mathrm{Re} \simeq \frac{UL}{\nu} \simeq \frac{L^2A^{2/3}}{\nu^{4/3}} = \mathrm{Re}_A^{4/3}, \qquad \nu_e \simeq \nu \mathrm{Re}_A^{2/3}. \quad (3)$$

To describe the wall layer, note that $v \equiv 0$ at a wall. Integrating Eq. (2) over y from wall to wall, we obtain that $\Omega(L/2) = -U'(L/2) = AL/2\nu$ is always equal to the laminar value; see the inset in Fig. 4(b). Now we estimate the width of the wall layer, $U/U'(L) \simeq LA^{2/3}\nu^{-1/3}/AL\nu^{-1} \simeq \nu^{2/3}/A^{1/3} \simeq \ell$, which confirms that Eq. (3) is self-consistent. Alternatively, one derives Eq. (3) by stating that the momentum flux is proportional to the velocity difference across the layer: $AL \simeq UU_\ell \simeq U^2\ell/L$.

The appearance of thin boundary layers at large Re (revealed in detail in the Supplemental Material [14]) must lead to a sharp maximum of the vorticity derivative: $\max \Omega_y \simeq \Omega(L/2)/\ell \simeq LA^{4/3}\nu^{-5/3}$, which is much larger than $\Omega_y(L/2) = A/\nu$, derived from Eq. (2) at a wall. Away from the wall layer, turbulence suppresses the mean vorticity gradient, as seen in the insets in Figs. 4(b) and 5(b).

Numerical simulations support Eq. (3); see Fig. 5. The scaling $\mathrm{Re} \propto \mathrm{Re}_A^{4/3}$ continues through both weakly and strongly fluctuating regimes, even though the proportionality constant slightly changes at the transition [see the inset in Fig. 5(a)]. The mean vorticity at the boundary layer also follows the scaling in Eq. (3), as seen in the inset in Fig. 5(b) plotted for the rescaled quantity $\tilde{\Omega}_y = \Omega_y(y)/\max \Omega_y = \nu\Omega_y/A\mathrm{Re}_A^{2/3}$. Since Eq. (3) follows from the spanwise structure, it holds approximately even for the broken train [the leftmost cross in Fig. 5(a)]; the breakdown increases the flow rate a bit, apparently by widening the jet.

Let us discuss the role of the turbulent fluctuations. Flow dissipates energy and enstrophy, and the viscous dissipation rate of the former is proportional to the latter: $\nu\langle|\nabla v|^2\rangle = \nu\langle\omega^2\rangle$. Law (3) gives the same estimate for the pressure work and the dissipation rate: $\nu\overline{\Omega^2} \simeq \nu U^2/\ell L \simeq A^{5/3}L\nu^{-1/3} \simeq A\bar{U}$—that is, the mean flow is able to dissipate energy by itself. Indeed, the DNS data in Fig. 4 show that turbulent enstrophy fluctuations are smaller than mean, while velocity fluctuations are negligible. Enstrophy dissipation is determined by the vorticity gradients shown in Fig. 5(b). The mean gradient follows Eq. (3), while variance (and the enstrophy dissipation) near the wall is much larger and grows with Re faster than the mean. The numerics thus confirm that the enstrophy is dissipated by turbulence rather than by the mean flow.

According to Eq. (3), the friction factor of the 2D channel, AL/U^2, decays as $\mathrm{Re}_A^{-2/3} \sim \mathrm{Re}^{-1/2}$, faster than in 3D, where one finds the empirical Blasius law $\mathrm{Re}^{-1/4}$ for moderate Re and the logarithmic decay for large Re. Such $\mathrm{Re}^{-1/2}$ scaling was actually observed in decaying grid-generated turbulence in soap film experiments and hypothesized to be related to enstrophy cascade [23]. Here we have shown that this law is quite universal.

The law (3) is expected to hold when the time of the momentum transfer to the wall, $U/A \simeq L(A\nu)^{-1/3}$, is shorter than the friction time α^{-1}; otherwise friction imposes a linear regime with $U \propto A$. This requires a force exceeding both viscous and friction thresholds: $A \gg \nu^2 L^{-3}$, $(\alpha L)^3/\nu$. We discuss briefly the role of the third dimension and the layer thickness h. For planar flows with an open top and no-slip bottom, $\alpha = 3\nu/h^2$, while vertical motions invalidate the very notion of α. An ability of moving walls to excite turbulence must depend on h: we expect turbulence when the wall Reynolds number Vh/ν becomes large. How wall-generated 3D turbulence will be distributed over a wide, thin channel deserves future studies, particularly on account of strong planar flows suppressing vertical motions [24]. For pressure-driven flows, the validity of Eq. (3) requires $\ell \simeq L\mathrm{Re}_A^{-2/3} = L\mathrm{Re}^{-1/2} \gg h$. As Re approaches $(L/h)^2$, we expect the decay of the friction factor with Re to slow down and eventually converge to the 3D values observed in rectangular ducts [25].

A traveling wave pattern thus enhances effective viscosity and suppresses the flow rate compared to the laminar regime. It is instructive to compare Eq. (3) with the enhancement of diffusivity κ by the factors $\mathrm{Pe}^{1/2}$ for cellular [26,27] and $\mathrm{Pe}^{1/3}$ for wall-attached flows [28], where $\mathrm{Pe} = UL/\kappa$. That enhancement leads to acceleration of flame fronts [29] and other phenomena. Similar to Eq. (3), interplay between small noise and advection universally leads to the $1/3$ scaling with noise amplitude: for the tumbling frequency of a polymer in a shear flow [30], or for the Lyapunov exponent of an integrable system under stochastic perturbation [31].

To conclude, wall-driven 2D flows relax to laminar at all values of viscosity and friction used. We described the traveling wave which replaces the pressure-driven laminar flow. In distinction from 3D, as the Reynolds number grows, the fluctuations increase, yet the mean flow preserves its traveling-wave "snake" form. A remarkable property of 2D snakes are separatrices, which modify momentum transport to the walls, leading to a new scaling law for the friction factor.

We thank A. Obabko for help in using `Nek5000`. The work was supported by the grants of the Minerva Foundation, ISF (No. 882), the RSF (No. 14-22-00259), and the NSF (No. DMS-1412140). Simulations are performed at Texas ACC using XSEDE, supported by NSF Grant No. ACI-1548562 through allocation TG-DMS140028.

[1] B. Eckhardt, T. Schneider, B. Hof, and J. Westerweel, Annu. Rev. Fluid Mech. **39**, 447 (2007).
[2] C. C. Lin, Proc. Natl. Acad. Sci. U.S.A. **30**, 316 (1944).
[3] S. Orszag and L. Kells, J. Fluid Mech. **96**, 159 (1980).
[4] H. Faisst and B. Eckhardt, Phys. Rev. Lett. **91**, 224502 (2003).
[5] H. Wedin and R. Kerswell, J. Fluid Mech. **508**, 333 (1999).
[6] B. Hof *et al.*, Science **305**, 1594 (2004).
[7] R. Hewitt and P. Hall, Phil. Trans. R. Soc. A **356**, 2413 (1998).
[8] Y. Couder, J. M. Chomaz, and M. Rabaud, Physica (Amsterdam) **37D**, 384 (1989).
[9] H. Kellay, X-l. Wu, and W. I. Goldburg, Phys. Rev. Lett. **74**, 3975 (1995).
[10] G. Falkovich, G. Boffetta, M. Shats, and A. S. Lanotte, Phys. Fluids, **29**, 110901 (2017).
[11] C. C. Liu, R. Cerbus, and P. Chakraborty, Phys. Rev. Lett. **117**, 114502 (2016).
[12] J. P. Rothstein, Annu. Rev. Fluid Mech. **42**, 89 (2010).
[13] R. Fjørtoft, Geophys. Publ. Oslo **17**, 1 (1950).
[14] See the Supplemental Material at http://link.aps.org/supplemental/10.1103/PhysRevLett.121.164501, which includes movies, for more details on the numerical procedure, transient evolution, and flow structure.
[15] J. Jimenez, J. Fluid Mech. **218**, 265 (1990).
[16] F. Mellibovsky and A. Meseguer, J. Fluid Mech. **779**, R1 (2015).
[17] S. A. Orszag, J. Fluid Mech. **49**, 75 (1971).
[18] M. Umeki, Fluid Dyn. Res. **13**, 67 (1994).
[19] A. Fortin, M. Jardak, J. J. Gervais, and R. Pierre, J. Comput. Phys. **115**, 455 (1994).
[20] A. Drissi, M. Net, and I. Mercader, Phys. Rev. E **60**, 1781 (1999).
[21] J. D. Pugh and P. G. Saffman, J. Fluid Mech. **194**, 295 (1988).
[22] G. K. Batchelor, J. Fluid Mech. **1**, 177 (1956).
[23] T. Tran, P. Chakraborty, N. Guttenberg, A. Prescott, H. Kellay, W. Goldburg, N. Goldenfeld, and G. Gioia, Nat. Phys. **6**, 438 (2010).
[24] H. Xia, D. Byrne, G. Falkovich, and M. Shats, Nat. Phys. **7**, 321 (2011).
[25] E. Fried and I. E. Idelchik, *Flow Resistance: A Design Guide for Engineers* (Hemisphere, New York, 1989).
[26] S. Childress, Phys. Earth Planet. Inter. **20**, 172 (1979).
[27] B. Shraiman, Phys. Rev. A **36**, 261 (1987).
[28] M. N. Rosenbluth, H. L. Berk, I. Doxas, and W. Horton, Phys. Fluids **30**, 2636 (1987).
[29] N. Vladimirova, P. Constantin, A. Kiselev, O. Ruchayskiy, and L. Ryzhik, Combust. Theory Modell. **7**, 487 (2003).
[30] K. S. Turitsyn, J. Exp. Theor. Phys. **105**, 655 (2007).
[31] K. Lam and J. Kurchan, J. Stat. Phys. **156**, 619 (2014).